ECS Transactions, 77 (3) 29-36 (2017)
10.1149/07703.0029ecst ©The Electrochemical Society

Nanoscale Spin-Transfer Torque MRAM Etching Using Various Gases

K. C. Yang[a], S. W. Park[b], H. S. Lee[c], and G. Y. Yeom[a,c]

[a] School of Advanced Materials Science and Engineering, Sungkyunkwan University, 2066, Suwon, Republic of Korea
[b] Samsung Electronics, San No. 16 Banwol-Ri, Taean-Eup, Hwasung, 449-711, Republic of Korea
[c] SKKU Advanced Institute of Nano Technology (SAINT), Sungkyunkwan University, 2066, Suwon, Republic of Korea

The magnetic tunnel junction (MTJ)-related materials were etched using He, Ar, and CO/NH_3 in an inductively coupled plasma etching system. When the MTJ materials were etched with He, the etch selectivities and the etch profiles of the etched MTJ patterns were significantly improved. The sputter etch characteristics were also investigated using the Stopping and Range of Ions in Matter (SRIM) simulation program. The results showed higher sputter etch selectivity of CoFeB over W using He than those obtained using Ar. Also He exhibited higher energy and narrower angular probability density function of the sputtered atoms. Also, by using He, similar to Ar, magnetic properties of the MTJ were preserved compare to CO/NH_3 due to no oxidation of magnetic materials.

Introduction

As the volatile dynamic random access memory (DRAM) device faces a physical limitation, new memory devices are actively investigated to solve this problem [1, 2]. Among them, spin transfer torque magnetic random access memory (STT-MRAM) has received a lot of attention because of its very high speed of device, endurance, low power consumption of device, and high density memory cell in addition to the non-volatility of information [3, 4]. Especially, the MTJ memory elements which consist of $Co_xFe_yB_z/MgO/Co_xFe_yB_z$ multilayer structure are the critical building blocks for high density magnetic random access memory with high tunneling magnetoresistance (TMR) [5-7]. However, the dry etching of MTJ stack with sub 70 nm is a challenging step in the fabrication of STT-MRAM [8]. The etching of nanoscale MTJ induces oxidation in magnetic layer, pattern degradation and damage, or sidewall redeposition with the slanted etch slope of the patterned MTJ sidewall [9]. The etch process using C-O based chemistry and halogen gas induces more magnetic degradation in magnetic tunneling junctions (MTJs) compare to Ar. However, Ar causes more sidewall re-deposition and has a lower etch selectivity compare to C-O based chemistry [10-12].

In this study, for successful etching of MTJ related materials, such as CoFeB, CoPt, MgO and a hard mask material such as W, inductively coupled plasma (ICP) etching using Ar, He, and CO/NH_3 were conducted. Etch characteristics of magnetic tunnel junction (MTJ) stacks masked with W were investigated precisely using field emission scanning electron microscopy (FE-SEM) and TEM (Transmission electron microscopy). Simulation of MTJ material and hardmask material was conducted with SRIM simulation

to understand the differences in the sputter etch rates of magnetic materials by those gases. In addition, the magnetic hysteresis curves were analyzed using a vibrating sample magnetometer (VSM). The results showed that, among the various gas combinations, the use of He gas improved etch selectivity of MTJ materials over W and also improved the etch profile of MTJ features. Also the He etch gas could be beneficial in reducing damage.

Experimental

Hardware

The ICP etch system used in this study is shown in Figure 1. As shown in this figure, one-turn inductive coil was wound around the ceramic chamber wall and plasma power at 13.56 MHz was supplied using a generator (ENI). Also, a separate 13.56 MHz rf power was applied to the substrate for rf biasing. For the effective etching of MTJ patterns, various etch gases such as He, Ar, and CO/NH_3 gas mixture were used. The gas flow rate of 50 sccm, the process pressure of 7 mTorr and the ICP power of 700 W were maintained in this experiment. Bias voltage was decided by the Stopping and Range of Ions in Matter (SRIM) simulation.

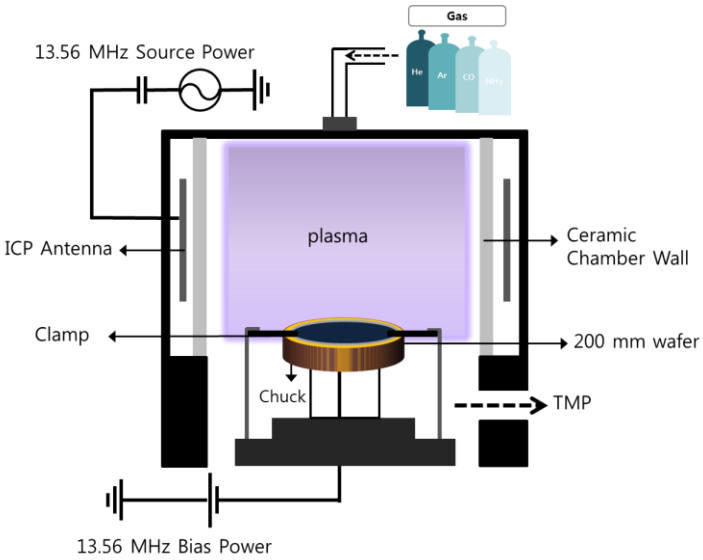

Figure 1. Schematic diagram of the ICP etcher used in this study.

Etch samples

For the etch samples, to measure the etch rates, MTJ related materials such as CoPt, MgO, CoFeB, and W deposited on silicon wafers were used. For the nanoscale MTJ feature etching, a MTJ stack of CoPt (10 nm)/MgO (1 nm)/CoFeB (10 nm) deposited on a $Ta/SiO_2/Si$ wafer and masked with a 55 nm width pattern composed of SiO_x, W, Ti and Ru was used as shown in Figure 2.

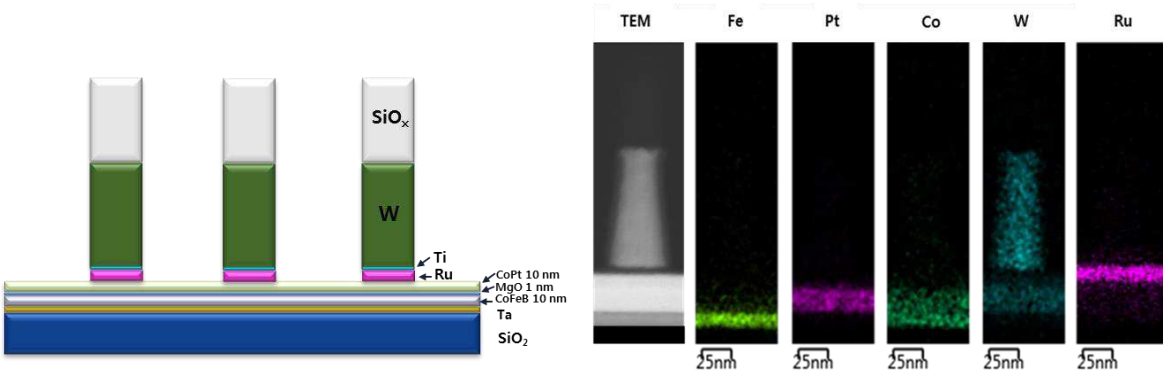

Figure 2. Schematic diagram of the MTJ stack and structure of the MTJs taken by transmission electron microscopy (TEM).

Characterization

After the etching of the MTJ-related materials and the hard mask material, a step profilometer (Tencor Alpha step 500) was used to measure the etch depth. The etch profile of the patterned MTJ stack was observed by using a field emission scanning electron microscope (FE-SEM, Hitachi S-4700). SRIM simulation was conducted to investigate the sputter yield <S> and the sputter etch selectivity over hardmask during sputter etching. The specific simulation conditions are described in Table I. As shown in Table I, the monolayer collision steps / surface sputtering calculation mode was used and, for CoFeB, the ratio of Co:Fe:B = 4:4:2 was used in this study. Analyses such as sputter yield selectivity, sputtered atomic angle, and energy distribution of sputtered atoms were also investigated using the SRIM simulation data.

TABLE I. SRIM input parameters for W and CoFeB (4:4:2). ρ is the bulk material density, E_D is the bulk atom displacement energy, E_L is the lattice energy, and U_0 is the surface atom binding energy. Each value was obtained from the reference and other values were used to deduce sputter yield and sputtered atom characteristics[13,14]

	Type of SRIM calculation	ρ (g/ cm^3)	U_0 (eV)	E_D (eV)	E_L (eV)	Ion incident energy (eV)
W	Monolayer collision steps / surface sputtering	19.35	25	3	8.68	He: 150/ 250 /350 Ar: 35/47/52
CoFeB (4:4:2)	Monolayer collision steps / surface sputtering	7.80	Co: 25 Fe: 25 B: 25	Co: 3 Fe: 3 B: 3	Co: 4.43 Fe: 4.34 B: 5.73	He: 150/ 250 /350 Ar: 35/47/52

Results and Discussion

The sputter yields of Co, Fe, and B in amorphous CoFeB were investigated using the SRIM program with the conditions in Table I and the results are shown in Figure 3. The ion energies of 150, 250, and 350 eV were used for He in the sputter etch simulation because the sputter threshold energy of W by He is in the range of 100-200 eV. Also the ion energies of 35, 47, and 52 eV were used for Ar, which showed a similar sputter etch rate range of magnetic materials to that by He ions. Although sputtering yield does not mean the etch rate of CoFeB, it has a proportional relation. As shown in Figure 3, the increase of He ion energy (150 → 350 eV) and Ar ion energy (35 → 52 eV) increased the CoFeB sputter yield values but, the sputter yield selectivity of CoFeB/W was decreased.

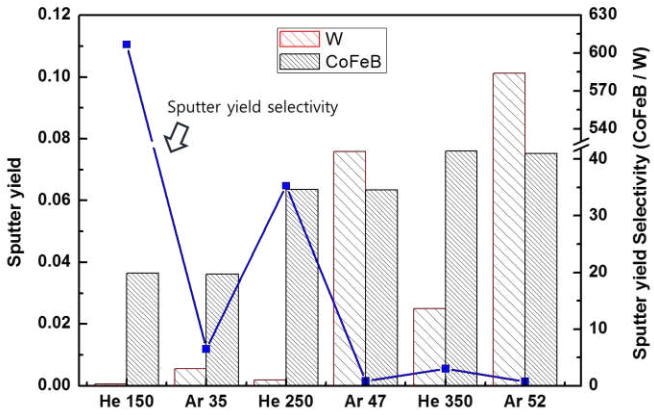

Figure 3. Sputter yield and sputter yield selectivity between CoFeB and W obtained by the SRIM simulation shown in TABLE I.

Also, we investigated, by measuring the sputtering yield of W and Fe in CoFeB both by experimentally and by simulation, the etch rates and etch selectivities of MTJ materials were compared for He and Ar. The simulation data showed that the sputter yield selectivity of W over CoFeB is much higher for He than Ar ion. Similar tendency was observed by experiments in Figure 4 using blanket thin film samples.

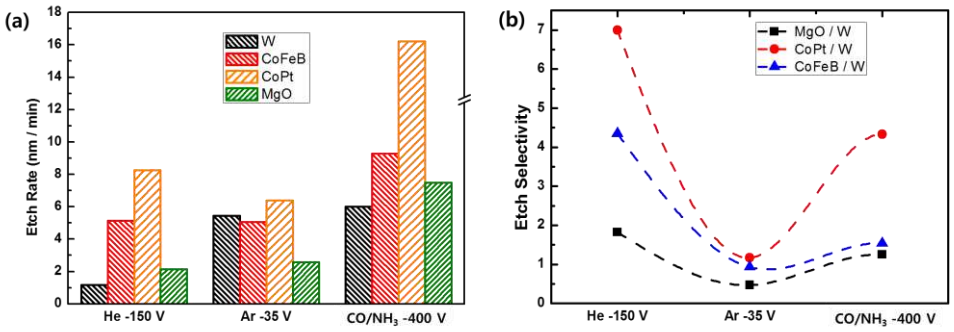

Figure 4. Etch rates of MTJ materials and W and etch selectivities of MTJ materials over W (a) etch rates of MTJ materials and (b) etch selectivities of MTJ materials over W.

Figure 4(a) shows the etch rates of CoFeB, CoPt, and MgO with W used as a hardmask material. Figure 4(b) shows the etch selectivities of the materials over W for etching using with a bias voltage of −150 V for He, −35 V for Ar, and −400 V for CO/NH_3 (1:3). The etch rates of CoFeB, CoPt, and MgO were generally similar for He and of Ar; therefore, the simulation results of sputter yields in Figure 3 could be confirmed experimentally. Also, the results of the etch selectivities followed the same trend, but the there were differences between the measured values and simulated data. We believe that it is related to the non-consideration of plasma potential, the energy distribution, the impurity effect, etc. that could not be considered in the simulation. Figure 5 (a), (b) show the simulation results of the energy and angular distribution of sputtered Fe in CoFeB and (c), (d) show the angular probability density function of sputtered Fe by 150 eV He ion and 250 eV He ion, respectively. The sputter angle and energy of magnetic materials during the etching could be related to the degree of sidewall-redeposition during the etching of nanoscale MTJ features which can affect the etch profiles and electrical short of MTJ. As shown in (a) and (b), 250 eV He has higher energy and higher ejection angle. Also, as shown (c) and (d), which was reconfigured from (a) and (b), average ejection angles for 150 eV He and 250 eV He were 17.13° and 18.07° from the vertical angle. The simulation results on behavior of Co and Fe were quite similar, therefore, only the results of Fe are shown in Figure 5 and Figure 6.

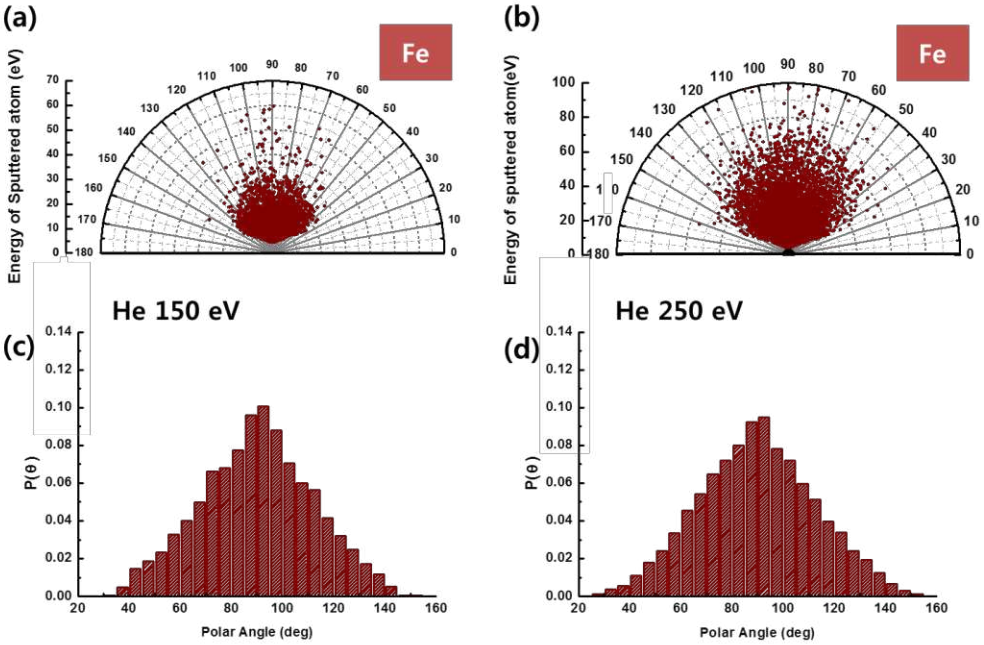

Figure 5. Energy and angular distribution of sputtered Fe in CoFeB with (a) 150 eV He ion and (b) 250 eV He ion by SRIM simulation. Angular distribution probability of sputtered Fe atom with (c) 150 eV He ion and (d) 250 eV He ion.

Figure 6 shows the simulation results of Fe by 35 eV Ar ion and 47 eV Ar ion, respectively. The average ejection angles for 35 eV Ar ion and 47 eV Ar ion were 20.53°

and 20.88° from the vertical angle, respectively. As shown in Figure 5 and 6, the sputtered Fe atoms tend to have higher energies for He compared to Ar.

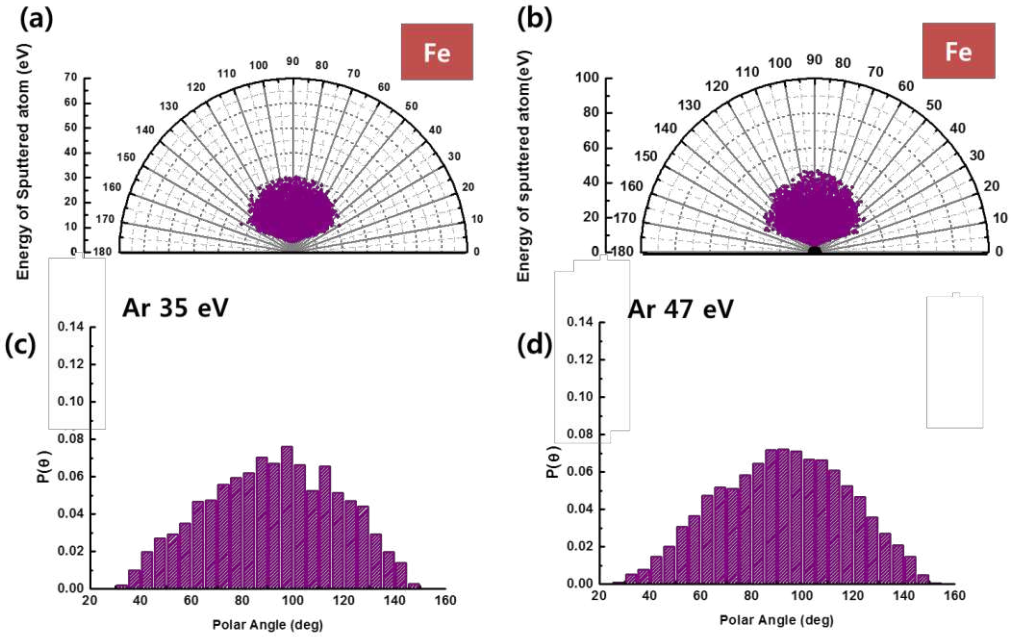

Figure 6. Energy and angular distribution of sputtered Fe in CoFeB with (a) 35 eV Ar ion and (b) 47 eV Ar ion by SRIM simulation. Angular distribution probability of sputtered Fe atom with (c) 35 eV Ar ion and (d) 47 eV Ar ion.

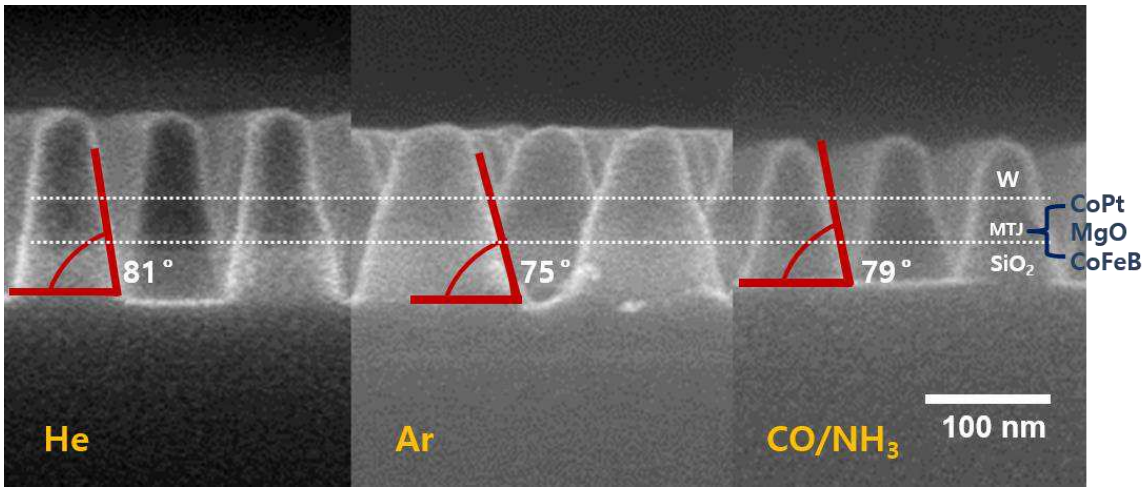

Figure 7. FE-SEM images of the etched MTJ patterns etched using the He, Ar and CO/NH_3 gases.

The etch profiles were observed by FE-SEM and the results are shown in Figure 7. When the nanoscale MTJ features were etched with He, Ar and CO/NH_3 gases, the use of pure

Ar gas degraded the W hardmask and increased the bottom width, so that the spaces between the MTJ features were filled with the redeposited materials, and which produced a slanted etch slope. On the contrary, when He and CO/NH_3 were used as the etch gases, the MTJ etch profiles were improved and the etch residue on the sidewall of the MTJ feature was decreased. Especially, the sidewall angle of the MTJ stacks was more anisotropic with He gas. As shown in Figure 7, the sidewall angles of the MTJ stacks were 81 degree for He, 75 degree for Ar and 79 degree for CO/NH_3.

,

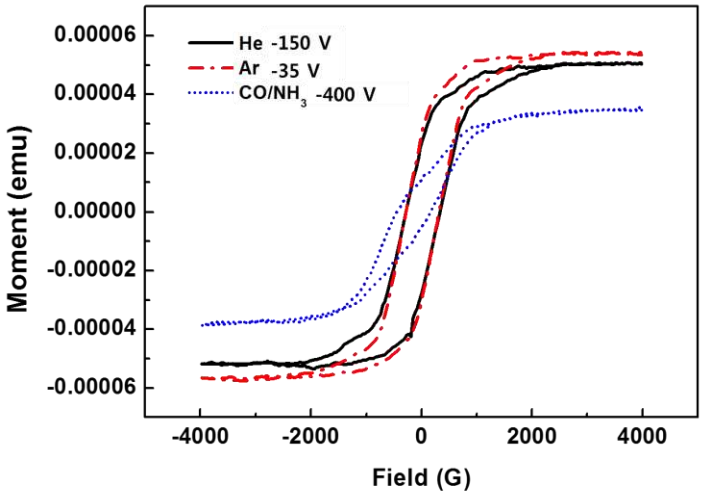

FIG. 8. Magnetization behaviors of patterned MTJs etched using He , Ar, and CO/NH_3.

In general, oxidation and damage of the magnetic layer are mainly associated with a magnetic degradation. So, to investigate the magnetic degradation of the MTJ features after the etching, minor magnetic hysteresis loops of patterned MTJ were measured by the VSM method. As shown in Figure 8, when a MTJ feature was etched with −150 V of He, the M_S was a little lower (92.3%) than that etched with -35V of Ar. However, in the case of the M_S of MTJ etched by -400V of CO/NH_3, it was 61.1% of that etched with Ar. The oxygen in the gas chemistry tends to form a thin oxide layer on the patterned sidewall of MTJ materials, which reduces the performance of the device.

Conclusions

The patterned MTJ exhibited a much better etch profile and less hard mask erosion by using He instead of Ar due to the higher etch selectivities of magnetic material over W for He compared to Ar at the similar etch rates of magnetic materials. In addition, magnetic materials sputtered by He were less re-deposited on the sidewall of the etched features especially at an He ion energy close to the hardmask sputter threshold energy. The use of CO/NH_3 gas mixture exhibited the etch characteristics comparable to He. However, the CO/NH_3 gas mixture appeared to induce more magnetic degradation than the inert gases such as He and Ar, possibly due to the chemical chemistry containing oxygen. Therefore, it is believed that the etching of nanosized MTJ pattern using He with the ion energy near the hardmask sputter threshold energy could be beneficial in

obtaining high etch selectivity over mask and high degree of anisotropy etch profiles without significant electrical degradation of magnetic properties.

Acknowledgments

This research was supported by the (NRF-2016M3A7B4910429).

References

1. J. H. Lee, *ECS Trans.*, **60**(1), 983 (2014).
2. F. Balestra, *ECS Trans.*, **66**(5), 211 (2015).
3. D. C. Worledge, M. Gajek, D. W. Abraham, S. Brown, M. C. Gaidis, G. Hu, J. Nowak, E. J.. O'Sullivan, R. P. Robertazzi, J. Z. Sun, P. L. Trouilloud and W. J. Gallagher, *4th IEEE International.*, (2012).
4. E. J. O'Sullivan, M. J. Gajek, J. J. Nowak, S. L. Brown, M. C. Gaidis, G. Hu, J. Z. Sun, P. L. Trouilloud, D. W. Abraham, R. P. Robertazzi, W. J. Gallagher and D. C. Worledge, *ECS Trans.*, **58**(5), 117(2013).
5. Yiwei Liu, Jingyan Zhang, Shouguo Wang, Shaolong Jiang, Qianqian Liu, Xujing Li, Zhenglong Wu and Guanghua Yu, *ACS Appl. Mater. Interfaces.*, **7**, 26643 (2015).
6. M. Zhu, H. Chong, Q. B. Vu, T. Vo, R. Brooks, H. Stamper, S. Bennett and J. Piccirillo, *Appl. Phys. Lett.*, **106**, 212405 (2015).
7. I. Barsukov, Yu Fu, C. Safranski, Y. J. Chen, B. Youngblood, A. M. Gonçalves, M. Spasova, M. Farle, J. A. Katine, C. C. Kuo and I. N. Krivorotov, *AppL. Phys. Lett.*, **106,** 192407 (2015).
8. Makoto Satake, Masaki Yamada and Eiji Matsumoto, *Vac. Sci. Technol. B.*, **34**, 061806 (2016).
9. Yuichi Ohsawa, Naoharu Shimomura, Tadaomi Daibou, Yuzo Kamiguchi, Satoshi Shirotori, Tomoaki Inokuchi, Daisuke Saida, Buyandalai Altansargai, Yushi Kato, Hiroaki Yoda, Tadakatsu Ohkubo and Kazuhiro Hono, *IEEE Trans. Magn.*, **52**(7), 3400803(2016).
10. K. Kinoshita, H. Honjo, S. Fukami, H. Sato, K. Mizunuma, K. Tokutome, M. Murahata, S. Ikeda, S. Miura and N. Kasai, Jpn. J. Appl. Phys. **53**, 103001 (2014).
11. K. Kinoshita, H. Utsumi, K. Suemitsu, H. Hada and T. Sugibayashi, Jpn. J. Appl. Phys. **49**, 08JB02 (2010).
12. M. H. Jeon, H. J. Kim, K. C. Yang, S. K. Kang, K. N. Kim and G. Y. Yeom, Jpn. J. Appl. Phys. **52**, 05EB03 (2013).
13. P. Kumar, A. Ahmad and M. Carrère, Radiat. Eff. Defects Solids. **170**, 567 (2015).
14. D. Kirk, A. Kohn, K. B. Borisenko, C. Lang, J. Schmalhorst, G. Reiss and D. J. J. Cockayne, Phys. Rev. B, **79**, 014203 (2009).